DOI: 10.13009/EUCASS2022-4634
9TH EUROPEAN CONFERENCE FOR AERONAUTICS AND SPACE SCIENCES (EUCASS)

Wind Tunnel Experiments of the CALLISTO VTVL Launcher in the TMK and HST Wind Tunnels

Johannes Riehmer[1], Kees Kapteijn[2], Josef Klevanski[3], Bodo Reimann[4], Sven Krummen[5], Ali Gülhan[6] and Etienne Dumont[7]

[1]DLR, Institute of Aerodynamics and Flow Technology, Supersonic and Hypersonic Technologies Department, Linder Hoehe, 51147 Cologne, Germany, Johannes.Riehmer@dlr.de

[2]DNW, Voorsterweg 31, 8316 PR Marknesse, The Netherlands, Kees.Kapteijn@dnw.aero

[3]DLR, Institute of Aerodynamics and Flow Technology, Supersonic and Hypersonic Technologies Department, Linder Hoehe, 51147 Cologne, Germany, Josef.Klevanski@dlr.de

[4]DLR, Institute of Aerodynamics and Flow Technology, Spacecraft Department, Linder Hoehe, 51147 Cologne, Germany, Bodo.Reimann@dlr.de

[5]DLR, Institute of Space Systems, Robert Hooke-Str. 7, 28359 Bremen, German, Sven.Krummen@dlr.de

[6]DLR, Institute of Aerodynamics and Flow Technology, Supersonic and Hypersonic Technologies Department, Linder Hoehe, 51147 Cologne, Germany, Ali.Guelhan@dlr.de

[7]DLR, Institute of Space Systems, Robert Hooke-Str. 7, 28359 Bremen, German, Etienne.Dumont@dlr.de

Abstract

CALLISTO is a demonstrator for a first stage of a reusable vertical take-off, vertical landing rocket and is developed and build within a collaboration of DLR, CNES and JAXA [1]. DLR is leading the aero science team [2] and is in charge of the aerodynamic and aerothermodynamic characterization of the vehicle. Within this task, experimental work has been carried out at two different wind tunnels on two different models in order to determine the aerodynamic coefficients and uncertainties for the AErodynamic Data Base (AEDB) of the vehicle with focus on the descent flight configuration.
First data was obtained in the Trisonic Wind Tunnel (TMK) at the DLR Department of Supersonic- and Hypersonic Flow Technologies in Cologne for a 1:35 model in a Mach number range from 0.5 up to 2.0. The second dataset was generated in the transonic wind tunnel (HST) of the DNW in Amsterdam for a 1:10 model in a Mach number range of 0.2 up to 1.3. Within this paper, the data from the two aforementioned facilities is compared with wind tunnel data of a simplified CALLISTO model [3,4,5] and the data [2] generated by numerical simulations. The results showed good agreement between the different facilities and datasets and was used to verify and improve the AEDB, especially in terms of uncertainties.

1. Introduction

The technology demonstrator CALLISTO is a joint project of CNES, DLR and JAXA and is aiming to develop and demonstrate VTVL technologies for future launch vehicles. In contrast to expendable rocket configurations reusable systems are exposed to a much broader variety of aerodynamic conditions especially during the descent phase. Therefore, a detailed aerodynamic analysis of all flight phases is necessary.
Within this study a detailed model (CAL1C) of the CALLISTO demonstrator including structural details like landing legs, fins, fittings, cable ducts and fluid lines was tested in two different wind tunnels at comparable conditions. This way it improves the level of detail from the previous investigations which was using a preliminary design iteration of CALLISTO labelled CAL1B [3,4,5]. The wind tunnels have been the Trisonic Wind Tunnel (HST) at the DLR Cologne and the High-Speed Tunnel at the DNW in Amsterdam. Since both wind tunnels are different in type, size and setup different models have been used.
For the experimental investigation the ascent (FFN – Folded Fins, Folded Landing Legs, No Thrust) and descent (UFN – Unfolded Fins, Folded Landing Legs, No Thrust) configurations of the CALLISTO flight demonstrator was tested. Hereby the focus was on the descent configuration with deployed fins, folded legs and without an engine plume. Since the wind tunnels are quite different each facility used a dedicated wind tunnel model. Main difference is the different scaling of the models whereas the reference geometry was identical in both cases.

DOI: 10.13009/EUCASS2022-4634

2. Methods

2.1 DLR Trisonic Wind Tunnel (TMK)

The DLR TMK wind tunnel is a blow down facility for Mach numbers between 0.5 and 5.7 and a test chamber with an area of 600x600 mm². For the test high pressure air from a pressure reservoir is released through a control valve into a settling chamber and into the test section. For subsonic to transonic conditions a constant area test section with perforated walls is used while for supersonic conditions an adaptable 2-D Laval nozzle is used to accelerate the flow to supersonic speeds before the test section. From the test section the air is guided into the free atmosphere via a diffusor and a silencer. For supersonic speed an ejector system can be used to decrease the backpressure and therefore decrease the Reynolds number. For subsonic conditions the static pressure has to be similar to the atmospheric pressure and variation of Reynolds number is only slightly possible by total temperature variation. Herby the capacity of the high-pressure reservoir restricts the time for each wind tunnel run up to 60 s depending on the flow conditions.

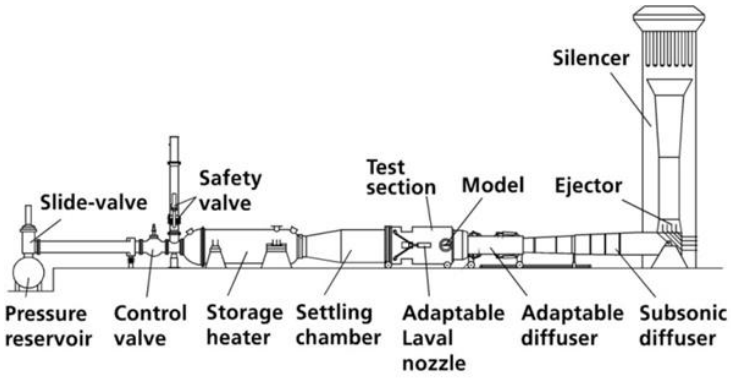

Figure 1: Schematic of the trisonic wind tunel TMK

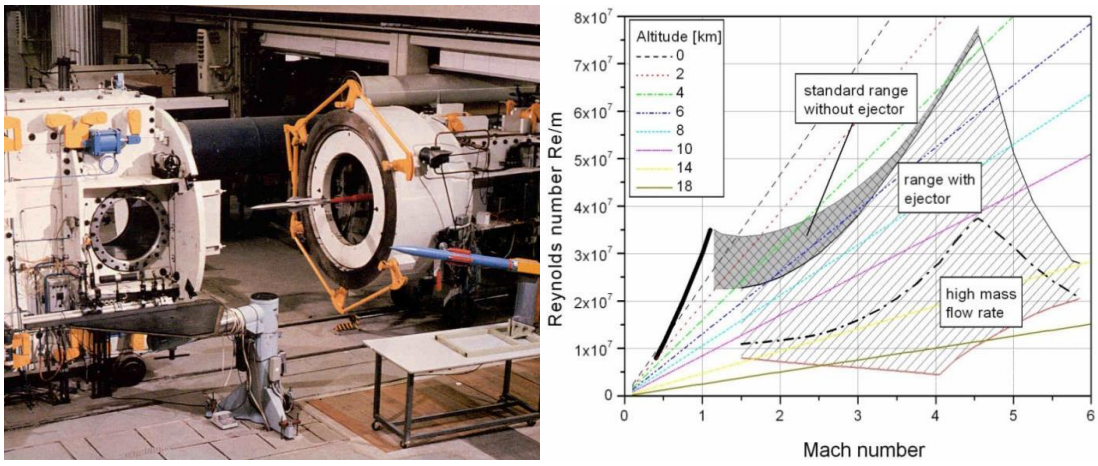

Figure 2: Test section (left) and performance chart (right) of the TMK wind tunnel

2.2 DNW High-Speed Tunnel (HST)

The High-Speed Tunnel (HST) of the German-Dutch Wind-tunnels (DNW) is a closed-circuit variable density continuous wind tunnel for subsonic, transonic and low supersonic wind speeds from Mach 0.15 up to Mach 1.35. The stagnation pressure can be varied between 20 and 390 kPa. An adjustable nozzle is followed by a test section with solid sidewalls and either slotted, perforated or solid movable top and bottom walls. The test section is significantly larger in comparison to the TMK with a width of 2 m. The adjustable top and bottom walls enable a test section height of 1.6 or 1.8 m. The actual measurements are achieved in a test section of 1.8 m height with slotted top and bottom walls.

DOI: 10.13009/EUCASS2022-4634

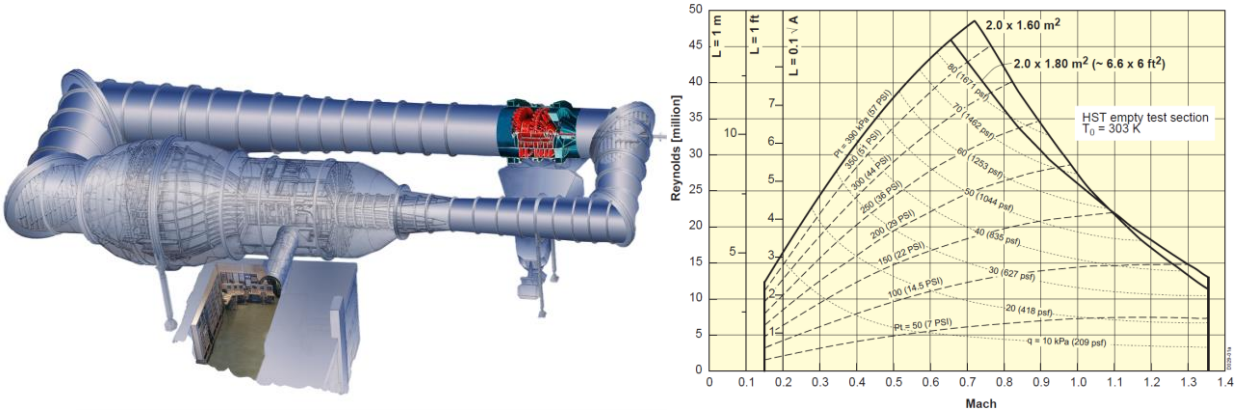

Figure 3: Schematic (left) and performance chart (right) of the HST wind tunnel

2.3 Wind Tunnel Models

The HST model (1:10) was significantly larger than the TMK model (1:35) with a length of 1.3 m and a diameter of 110 mm in contrast to 0.37 m length and a diameter of 31 mm for the TMK model. Due to the larger scale the CALLISTO layout could be reconstructed in higher detail for the HST model. In particular the external fluid lines and the struts of the landing leg assembly of the rocket have been integrated similar in the HST model, while for the TMK model they have been extruded from the body of the model. Also, the fins could be individually adjusted for the HST model while the TMK model used a replaceable fin section. In Figure 4 a drawing of both models is shown side by side. Slight differences can be seen on the struts of the landing legs and on the attachments of the fluid lines.

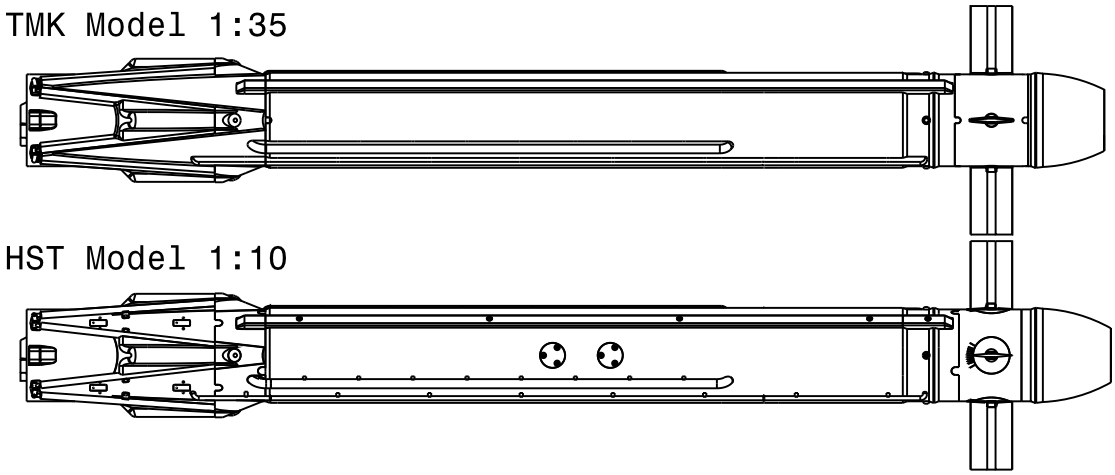

Figure 4: Comparison of the TMK and HST model in UFN configuration

The wind tunnel models have been designed in order to allow the mounting of the model in forward (FFN) and backward (UFN) flight direction. A balance mounting was in the middle of the model and could be inserted from the front of the vehicle for the UFN configuration and from the back of the vehicle for the FFN configuration. In Figure 5 the both configurations are shown implemented in the different wind tunnels. Since different wind tunnels, models, balances, and stings have been used the diameter of the cutout for the sting are different for both wind tunnels. Especially, for the backwards flying UFN configuration this cutout and the attached sting has a significant influence on the flow separation on the tip of the vehicle.

To measure static forces and moments both models were equipped with a balance which measured the six force and moment components with strain gauges. The balances have been chosen to be compliant with the loads occurring at maximal stagnation pressure and an angle of attack of 10°. For certain conditions the loads needed to be reduced to avoid damage of the model in the wind tunnel.

Additional measurements have been static pressure measurement in the base region of the model and dynamic pressure measurements in the base and landing leg region of the vehicle, but within this paper the pressure measurements are not considered.

DOI: 10.13009/EUCASS2022-4634

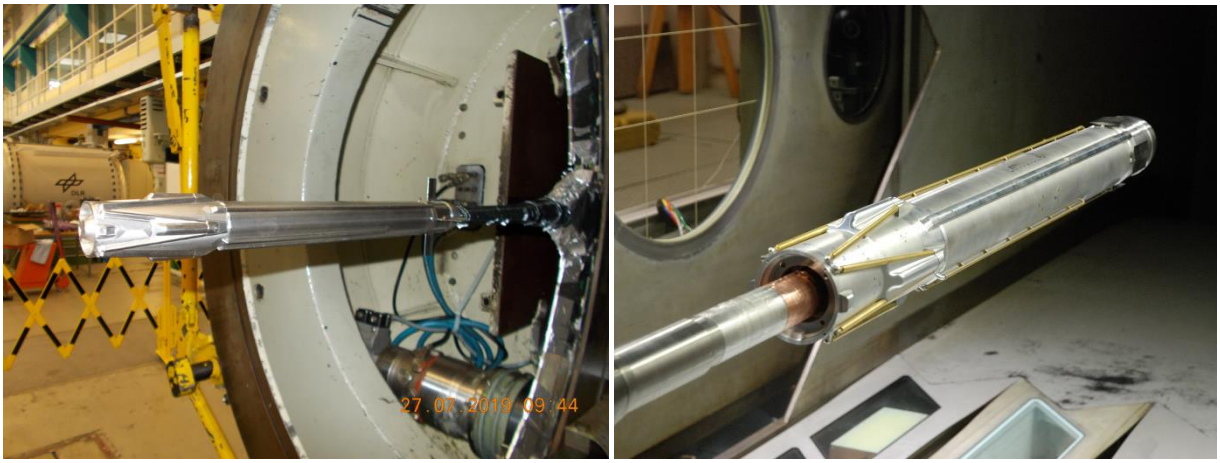

Figure 5: Model integrated in the TMK (left; UFN) and HST (right; FFN) wind tunnel

2.4 Reference frame and test procedure

The reference frames used with in this paper is taken over from the coordinate system defined for the CALLISTO flight vehicle. The main reference frame is sketched in Figure 6 and labeled with the index "TAU". It is a body fixed system with the main x-axis aligned in the rotational axis of the vehicle and the y-axis in direction of fin 1. The angle of roll is denoted with φ and can be seen in the figure as well. Within this paper the angle of attack α is always referring to the total angle of attack (α_s in Figure 6) and is the angle between the x-axis of the reference frame and the global flow vector. The numbering and fin deflection orientation can be seen in the right picture of Figure 6.

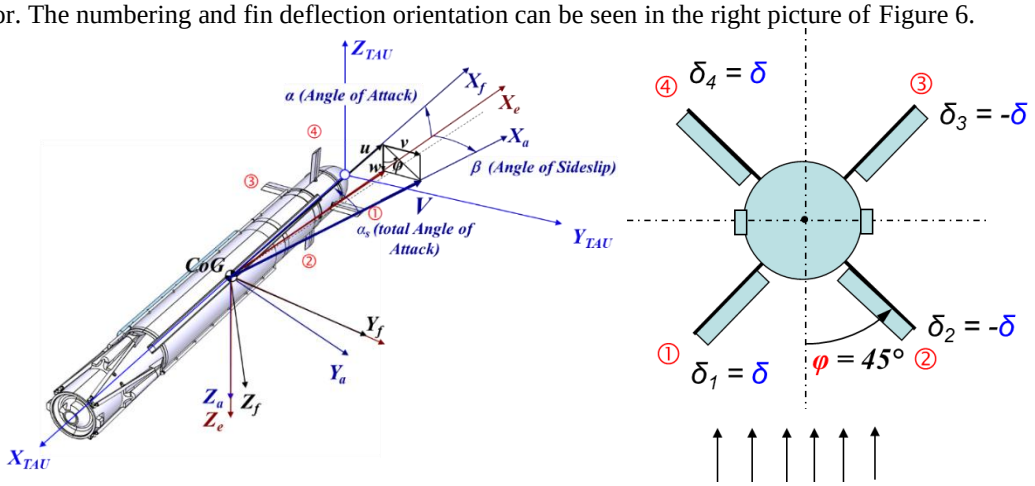

Figure 6: Reference frame and fin labeling

Since the wind tunnels are slightly different from each other the test procedure was different for the wind tunnels. For a typical run in the TMK the model was aligned in an angle parallel to the incoming flow. Than an angle of attack swept from 0° to -10° to +10° and back to initial position was performed with a rate of 2°/s. Data sampling rate was at 500 Hz to detect in-stationary effects but for visualization it was digitally filtered to 1 Hz. For different configurations and fin deflections the model was partially disassembled and reintegrated between the different runs. For different roll angles the model was rotated on the balance.

As the HST is a continuously operated wind tunnel it has, beside the possibility to sweep through the angle of attack, the possibility to roll the model with the balance within 360°. This way the angle of attack and roll of the model can be continuously varied during the runtime of the test. The sweep rate for the angle of attack was between 0.3°/s (subsonic), 0.2°/s (transonic) and 0.1°/s (Mach 1.29) while it was 4.4°/s for angle of roll. The increment between data points amounted to 0.2° in angle of incidence direction and 2.6° in roll direction. An analogue data filter at 1 Hz low pass was employed. For the HST tests it was originally foreseen to get a full roll polar for two different angles of attack and angle of attack polars for every 45° roll angle. With this test procedure the full characterization of one Mach number would have taken quite long and not all intended Mach numbers and model configurations could have been analyzed. Therefore, this procedure was manually optimized to measure some essential points for reconstruction of the α-φ plane together with only a few α and φ polars, and this way to reduce the runtime for each Mach number

DOI: 10.13009/EUCASS2022-4634

significantly. In Figure 7 on the left a sample test procedure for HST is shown while on the right side the procedure for the TMK is shown. This pattern of polars was processed for each Mach number. After completion of one Mach number the conditions were changed to another Mach number or Reynolds number without shutting down the wind tunnel.

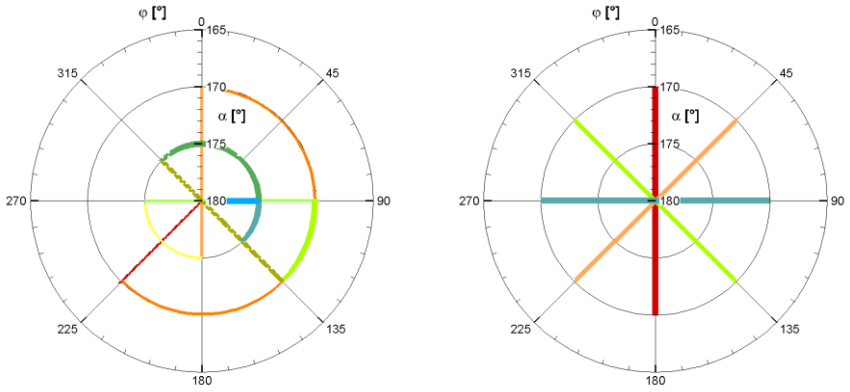

Figure 7: Test procedure for HST (left) and TMK (right) during a single Mach number run

For changing the fin deflection or switching the model from UFN to FFN in both wind tunnels the operation was stopped and modifications on the model were performed.
In Figure 8 the investigated Mach numbers and Reynolds numbers for both wind tunnels are plotted together with a generic trajectory for CALLISTO used as a reference. Both wind tunnels are not able to fully reproduce the flight conditions of the actual flight in terms of Mach number and Reynolds number. Especially the Reynolds number in the wind tunnels is significantly lower than for the descent flight. For the HST test campaign beside the conditions with maximal Reynolds number (label: HST) an additional sett of conditions for low Reynolds number was defined (label: HST 2) in order to investigate the Reynolds number effect and to have conditions comparable to the TMK conditions.

M	TMK	HST	HST 2
	Re [-] 10^6		
0.20	-	1.81	0.14
0.30	-	2.66	0.22
0.50	0.38	4.10	0.32
0.70	0.57	3.46	0.45
0.80	-	2.59	-
0.90	1.04	2.31	0.57
0.95	-	2.21	-
1.05	-	1.79	-
1.10	1.04	1.70	0.81
1.30	1.15	1.15	-
1.5	1.11	-	-

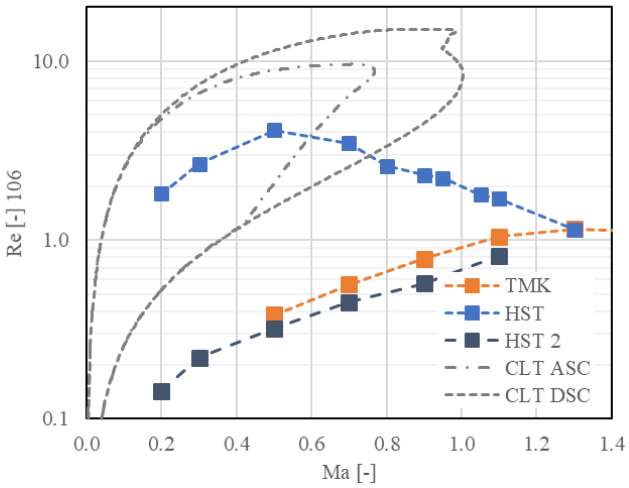

Figure 8: Reference trajectory and wind tunnel conditions

2.4 Uncertainties, AEDB and CFD

Uncertainties of the measurements have been calculated based on the measurement uncertainties of the balance components and the uncertainties of the pressure measurements of the wind tunnel and are therefore uncertainties of the measurement and do not include systemic errors. The uncertainties of derived quantities have been calculated using classical error propagation methods.
Additional to the measured data, data from the aerodynamic database (AEDB) composed by DLR [2] within the CALLISTO project is plotted within the graphs. Hereby, the actual parameter and the uncertainties are included, which refer to the general uncertainty regarding the repressiveness of the model with respect to the final flight configuration

DOI: 10.13009/EUCASS2022-4634

and not to a measurement uncertainty. At the current state the AEDB is made for real flight conditions along the trajectory (especially with respect to Reynolds number) and does not include an altitude dependency. Finally, some datapoints from high fidelity numerical RANS simulations (CFD) are usually shown within the following plots.

3. Results and Discussion

A total of around 580 drag polars for the HST and 120 for the TMK have been created during both test campaigns. Within this paper exemplary data will be presented to show the main aerodynamic characteristics for the UFN and FFN configuration for varying angle of attack, roll and Mach numbers. Hereby the focus is on the comparison of the different data sources and the uncertainties of the different approaches. Due to the large database this paper focus on a critical flight point at Mach 0.9 and 0° of roll angle. This point was selected as it is close to the transonic Mach number which was from greater interest, and also a large database from numerical simulations and the individual experiments was available for this configuration. As an angle of attack a value of 10° was chosen to get a reliable value for the center of pressure which is often used for vehicle characterization. Typically, a high Reynolds number of the HST (label: HST) and a low Reynolds number (label: HST 2) is shown together with data from the TMK (label: TMK) which was obtained for a comparable Reynolds number condition of the HST with low Reynolds number. For comparison data from the aerodynamic database for the flight vehicle (label: ADB) and numerical data from high fidelity RANS simulations (label: CFD) are plotted. Hereby, the latter two are for real flight conditions which derive in the Reynolds numbers in comparison to the experimental data (see Figure 8).
As indicators the main coefficients are plotted in the body fixed (c_x and c_z) and aerodynamic (c_d and c_l) coordinate system. The lift-to-drag ratio (L/D) is derived from the aerodynamic coefficients as well as the center of pressure. Hereby the full size of the vehicle is used for normalization.

3.1 UFN

The UFN configuration denotes the backwards flying configuration of CALLISTO and is of major interest since it is significantly different from traditional rocket configurations. The blunt base plate of the rocket causes a large stagnation region in front of the rocket which deflects the flow away from the rocket and later reattaches to the body base. This can be a source of large separation bubbles and in-stationary effects which can cause high structural and thermal loads and are typically hard to predict numerically as well as experimentally. The surface of the CALLISTO flight vehicle is also very complex due to the external fluid lines, different tank sections, cable ducts, fittings and the landing legs. In general, the shape is very complex in comparison to traditional rockets and causes not only a higher drag but also a higher uncertainty due to the more complex local flow phenomena and flow interactions. Additionally, these effects may cause unexpected side forces and moments which may affect the overall stability or controllability of the vehicle.
The complex and distorted flow on the base and main body impacts also the control surfaces (fins) which are essential for the stability and controllability of such a vehicle especially during the unpowered guided phases of the descent. Since this is a different flow field to an undisturbed flow the following sections will also have a closer look on the behavior on the usability of such control elements. For all other plots the fins are in an undeflected position.

Angle of Attack – Polar

The α-polar is the basic polar created in both wind tunnels at Mach 0.9 and 0° roll angle. Hereby the angle of attack was continuously varied from -170° to 190°. Under certain lower load conditions, the range was extended to higher angles of attack

DOI: 10.13009/EUCASS2022-4634

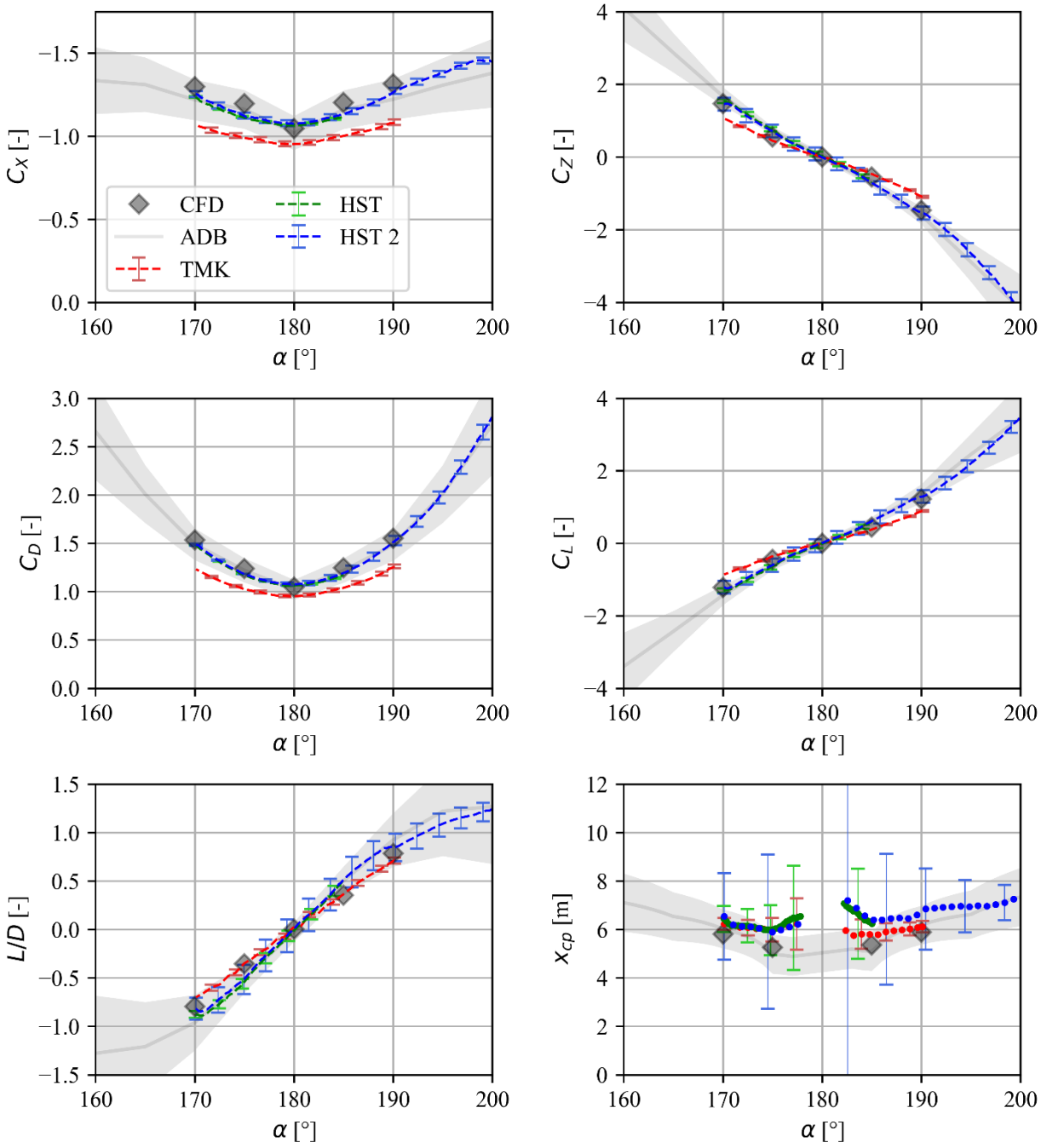

Figure 9: UFN α-polar for φ=0° at Ma=0.9

In Figure 9 such polars are plotted for the Mach 0.9 case at a roll angle of 0°. It can be seen, that all parameters are comparable between the different wind tunnel measurements and follow the trends predicted by the AEDB within the uncertainties. The TMK measurements are showing an offset in the drag coefficient C_D (respectively C_X) value. The reason for this cannot be directly deduced from the measurements and data. The slightly different geometry of the wind tunnel models seems to be the most plausible cause for these differences via the following effects:

- The more mechanical detailed HST model creates more drag on its protrusions in contrast to the TMK model which had to be simplified to be further manufacturable and has therefore a smoother surface.
- The sting for the balance of the TMK model was slightly larger than the sting for the HST model. This led to a different separation region behind the model and could affected the base pressures and consequently the base drag of the different models.

DOI: 10.13009/EUCASS2022-4634

Also, the slope of the lift coefficient c_l (respectively C_Z) is smaller for the TMK polar. The same reason as for the drag coefficient seems to be plausible here as well. When normalizing this coefficient with the drag coefficient by obtaining the lift-to-drag ratio (L/D) this discrepancy is reduced. The final plot in the bottom right of Figure 9 showed the center of pressure, whereas measurements close to 180° have been clipped to avoid division by zero. A good comparison between CFD, AEDB and the measurement is achieved. Nevertheless, the differences between the different datasets are significantly higher and also not symmetrical. Also, the error bars of the measurements are quite high and rise in proximity to 180° due to the numerical singularity. The measurements itself seem to be more accurate than the uncertainty analysis insists. A more detailed uncertainty analysis could therefore increase the reliability of the data. Generally, the data shows, that the determination of center of pressure is afflicted with a significant uncertainty.
Most notable for all graphs is the nearly identical lines of HST measurements which is on the one hand for the high Reynolds number condition (HST: green) and on the other hand for the low Reynolds condition (HST 2: blue). This leads to the conclusion, that the coefficients are minor affected by the Reynolds number in the investigated regime and allow a certain extrapolation of the test results to the real flight vehicle which can also be seen when comparing the experimental data with the numerical and the AEDB data.

Mach – Polar

The Mach polar was created by extracting single points for a dedicated angle of attack of α=170° and roll angle of φ=0° out of a α-polar and plotted together in the graphs of Figure 10. Again, a good comparison of measurements and predicted results from the AEDB and CFD could be observed.

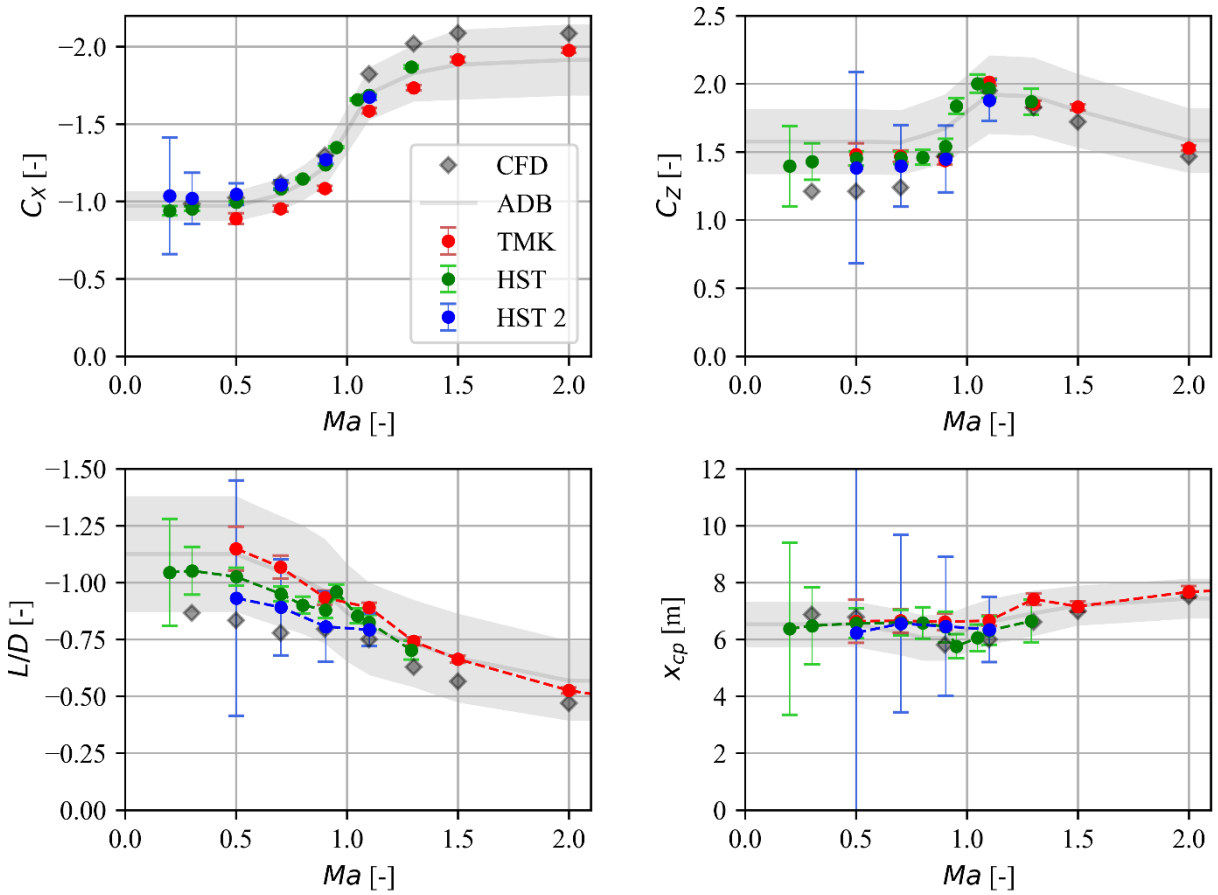

Figure 10: UFN Ma-polar for α=170° and φ=0°

The shape of the drag coefficient of Mach number is depicted quite similar for all datasets, whereas a small offset which is constant along the Mach number between the different curves can be found. The numerical simulations predict a slightly larger drag, while the TMK measurements are lower than the AEDB data and HST measurements. Which was already pictured in the α-polar (Figure 9). The Reynolds number variation measurements in the HST showed no significant influence on the drag coefficient.

DOI: 10.13009/EUCASS2022-4634

The lift coefficient is quite constant along the Mach number with a peek around the transonic regime and varies in a similar range between the different datasets. Again, the calculated uncertainties for the lift coefficient are quite high which effects also the derived parameters like lift-to-drag ratio or the center of pressure. Especially for the HST test the uncertainties rise with low Mach numbers and low Reynolds numbers. Since the measurement focused on the transonic regime and on high Reynolds number (high dynamic pressure) and not on low dynamic pressure conditions this is due to the low forces which the balance was not sized for. But since the measurements and other databases are quite close to each other it is very likely that the used uncertainties are significantly lower than the uncertainties shown in the analysis.

Roll – Polar

The φ-polar was generated also for the Mach 0.9 condition and an angle of attack of 170°. For the HST measurements different partial φ-polars have been concatenated while for the TMK data the individual points have been extracted out of α-polars. Similar to the other graphs the data is very comparable for the different data sources with an offset in the drag coefficient for the TMK measurements.

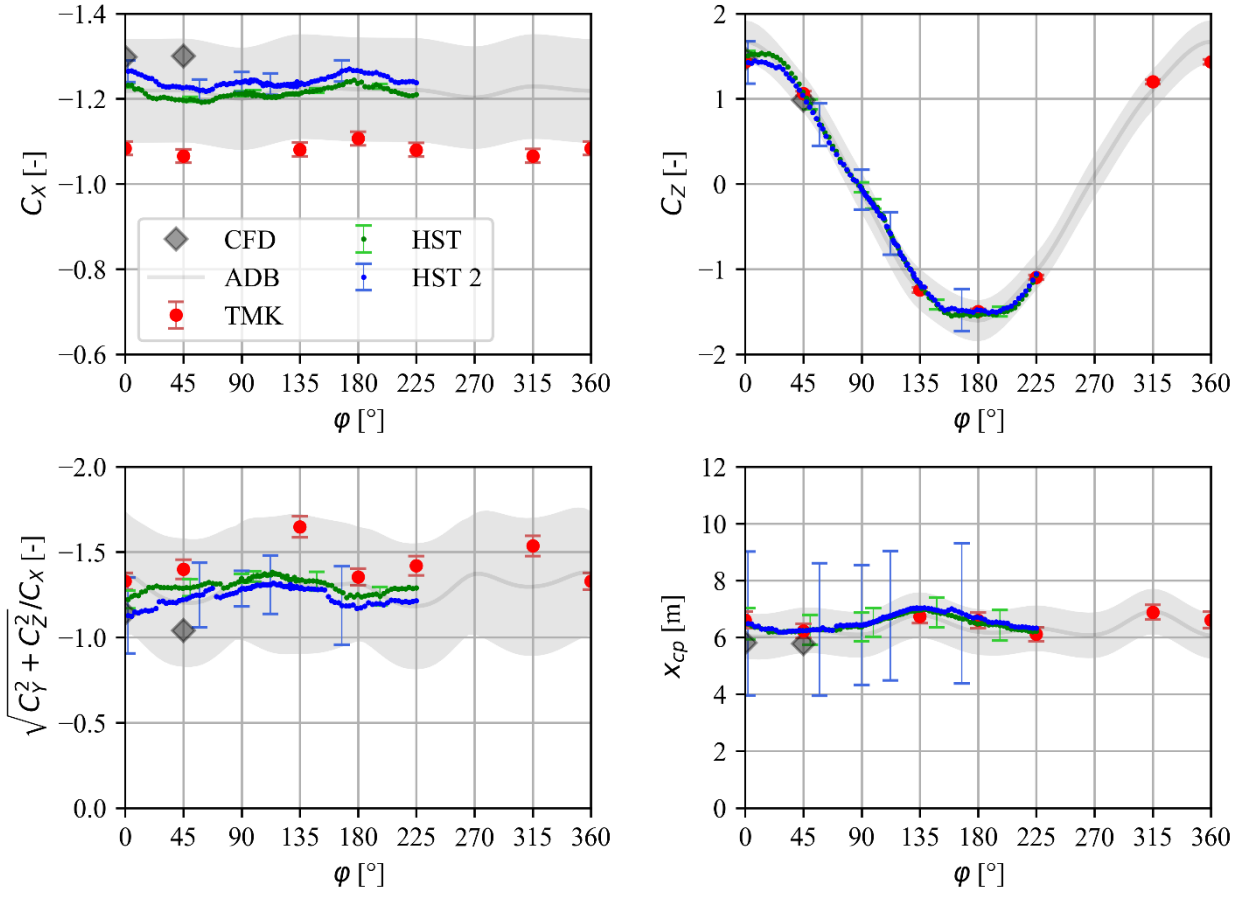

Figure 11: UFN φ-polar for α=170° at Ma=0.9

The drag coefficient only varies slightly with different roll angles and all measurements show a similar variation with increasing roll angle. Same behavior is observed for the lift coefficient with a good agreement for all datasets. In order to visualize the lift-to-drag ratio a different formulation for simplification was used (lower left of Figure 11). This relation of the axial forces to the lateral forces in the body fixed coordinate system shows similar curves for all data but with a relatively noisy dependency on the roll angle. The final plot shows the variation of the center of pressure which fits again quite well and show the same shapes for the AEDB and the measurements of both wind tunnels and different Reynolds numbers. Herby the center of pressure lies between 6.2 m and 7.1 m. Even that the uncertainty for the low Reynolds number is much higher it is indistinguishable from the more accurate high Reynolds number plot and confirms the assumption that Reynolds number effects are a minor influence parameter.

DOI: 10.13009/EUCASS2022-4634

Fin Deflection Impact

Various combination of fin deflection and flow states have been investigated. Within this section first the deflection of one single fin (fin 1, see Figure 1) at -10° and +10° are compared with the undeflected case. The reference case was an α-polar at Mach 0.9 and a roll angle of 0°. In order to reduce the presented data, CFD results are shown only for the case without deflection. The pitching moment for an arbitrary center of gravity at $7 \cdot x_{ref}$ (7 caliber) is plotted in the left of Figure 12 while the roll moment is plotted in the right chart. A negative deflection from the TMK measurement was not available. A good agreement between TMK and HST measurements could be achieved for both moment coefficients and showed a similar behavior as the AEDB data. The moments itself are very "bumpy" but allow in principle the stabilization of the vehicle for the specified center of gravity.

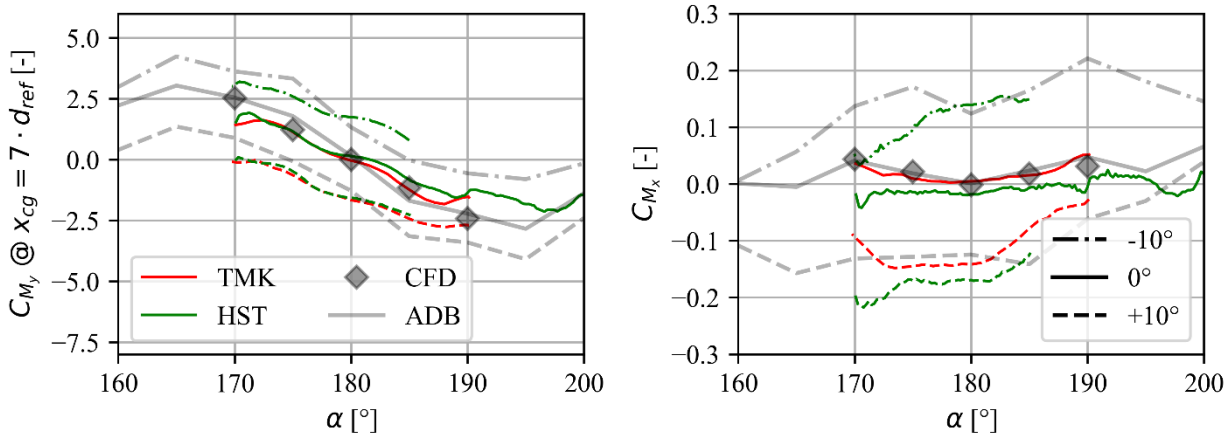

Figure 12: Influence on single fin deflection

Since a single fin deflection causes a change of multiple moments at once the vehicle will most likely controlled by the symmetric or anti-symmetric deflection of a pair or more fins in order to reduce buildup of multiple control moments and reduce it to a single main control moment. In order to investigate this behavior figure shows the symmetric deflection of fin #1 and #3 which can be used to control the pitching of the vehicle and therefore the global angle of attack. Hereby the deflection of the fin #1 is 0°, 10° and 20° while the deflection of fin #3 is 0°, -10° and -20° (see Figure 6). In these plots no deflection of 20° was available for HST. As it would be expected the pitch moment is nearly doubled for a 10° deflection of two fins in comparison to the single fin deflection of 10° whereas the roll moment is nearly unchanged. By increasing the deflection to 20° a flow separation is observed in the TMK data since the pitching moment is not doubled. Since the TMK data is a α sweep it can be seen that a flow separation occurred at 175° for a fin deflection of 20° resulting in a flow separation at 15° local angle of attack of the fin with respect to the global flow.

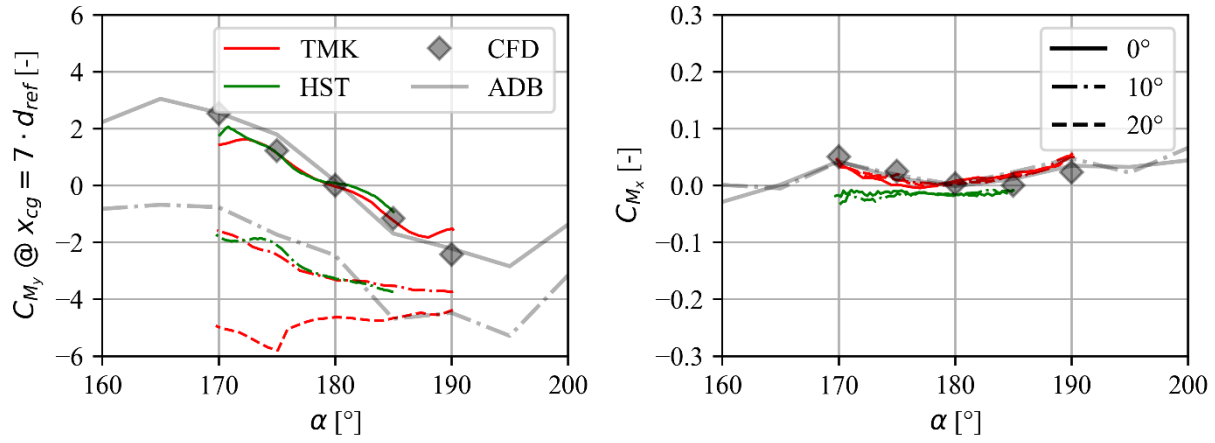

Figure 13: Influence on coefficient on symmetric# fin deflection

In comparison to Figure 12 no significant roll moment is induced. Nevertheless, a minor roll moment is to be expected and the different data sources predict different signs for that moment. Therefore, a small roll motion cannot be predicted from numerical nor experimental data.

DOI: 10.13009/EUCASS2022-4634

3.1 FFN

The FFN configuration is from interest for the ascent phase of the CALLISTO flight experiment. Especially together with the base pressure measurement the aerodynamic coefficients for the powered configuration (FFO) can be extrapolated. Also, since it is more comparable to classical aerodynamic configuration it is a good reference case to validate the measurements and compare it to the more complex UFN case. In the following paragraphs the same investigations as for the UFN case are presented except for the deployed fin configurations, since no ascent with deployed fins was foreseen at the time of investigation.

Angle of Attack – Polar

The angle of attack polar shows a similar behavior to the UFN case and is plotted in Figure 14. The drag is nearly reduced by a factor of two because of the more aerodynamic shape of the nose, whereas the lift to drag ratio is very comparable and the center of pressure is moved in a more forward position.

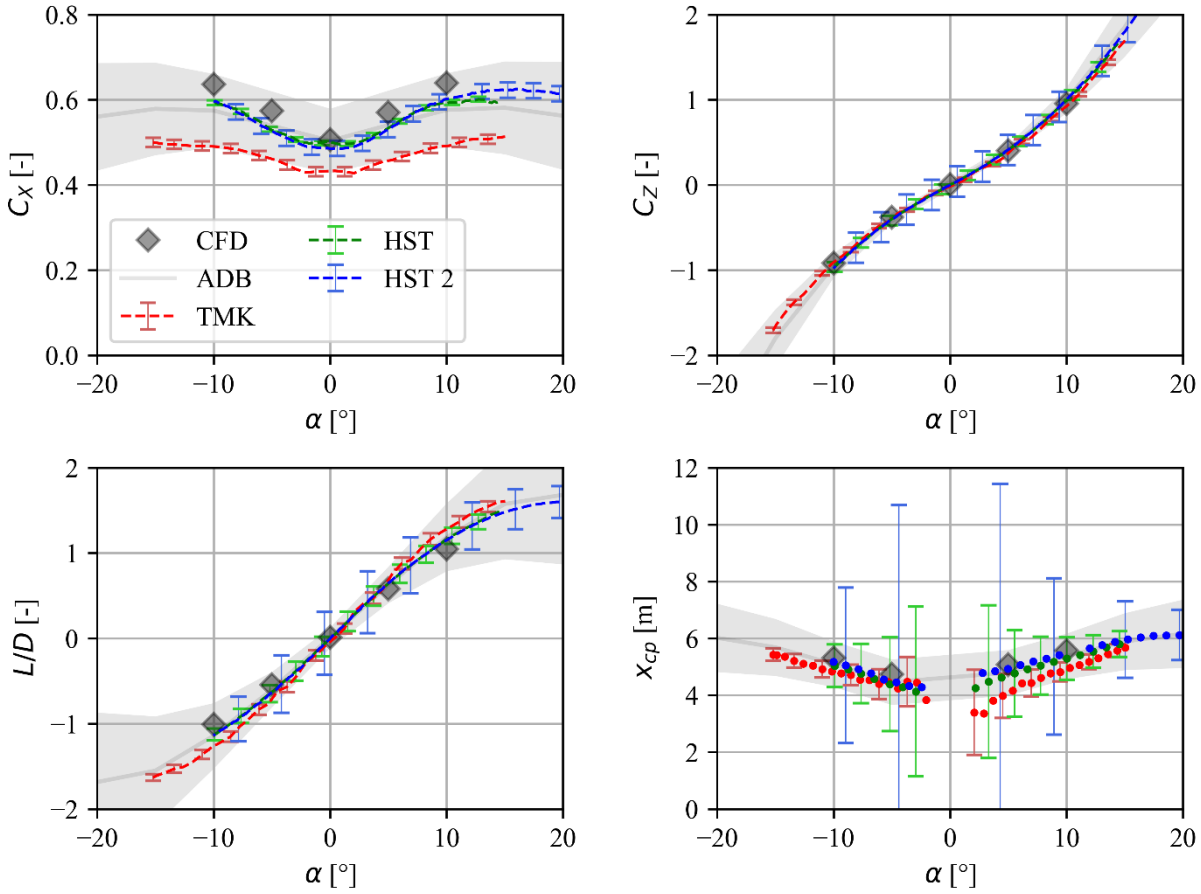

Figure 14: FFN α-polar

The effect of Reynolds number variation, performed in the HST campaign, was again neglectable for this configuration. Also, it can be seen that the data fit quite well with the numerical data and the aerodynamic database. The TMK measurement shows again a slightly lower drag coefficient. At 0° angle of attack this value is 10% lower than the HST value which is a comparable value as it can be observed for the UFN configuration. Since for the FFN configuration the flow on the base region separates very comparable at the edge between base plate and fuselage for both wind tunnel models the sting influence should be a minor influence factor here. As stated in section of the alpha polar of the UFN configuration multiple reasons for the deviation between TMK measurements and HST measurements are plausible and the current database is insufficient to deduce a certain factor, so a more detailed numerical or experimental analysis is required. The remaining parameters are in a very good agreement between all experimental data, the aerodynamic database and the numerical simulations and show less discrepancies as for the UFN configuration.

DOI: 10.13009/EUCASS2022-4634

Mach – Polar

The drag coefficient for the Mach polar of the FFN configuration (forward flight) is nearly half of the drag for the UFN configuration (backwards flight) even over the rise in the transonic regime. The data of all wind tunnel measurements and the CFD are within the uncertainties proposed by the AEDB. Whereas the TMK measurements show an underestimated drag in the subsonic regime this discrepancy vanishes in supersonic regime. As already observed in the angle of attack polar for FFN the discrepancies of the other parameters are lower than for the UFN configuration and lay within the uncertainties given by the AEDB.

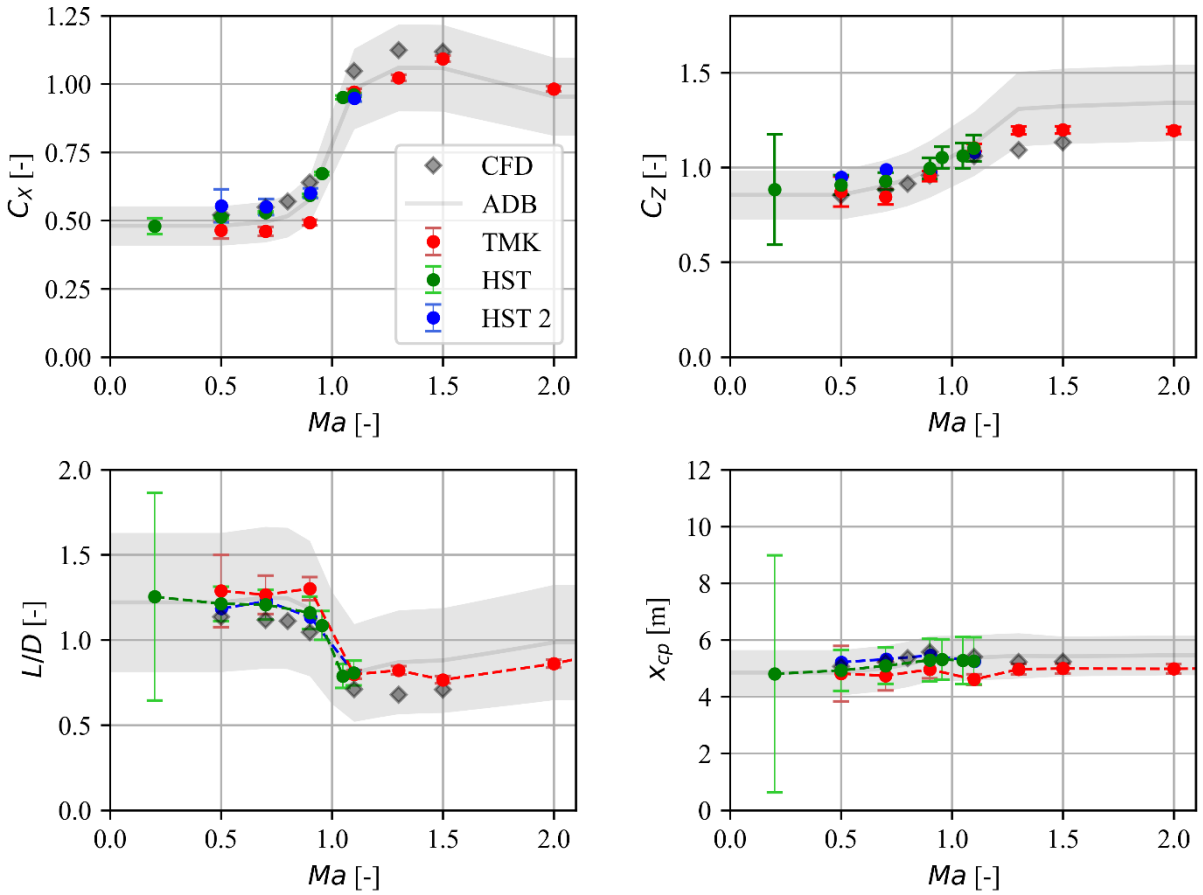

Figure 15: FFN Mach polar

Roll – Polar

The roll polar for the FFN configuration is nearly identical with the findings of the UFN configuration. Due to the the fittings, folded fins, protrusions, and cable ducts, the lift coefficient depends measurable on the lift-to-drag ratio while the drag itself is nearly constant. Hereby, the lift-to-drag value varies in a range of ±20% depending on the local roll angle. Also, the center of pressure moves by 0.5 m depending on the roll angle, which is significantly more constant as for the UFN configuration which changes in a range of 0.9 m. Especially, when comparing the different Reynolds numbers of the HST wind tunnel, which are nearly identical, the assumption of a neglectable Reynolds number influence can be verified once more.

DOI: 10.13009/EUCASS2022-4634

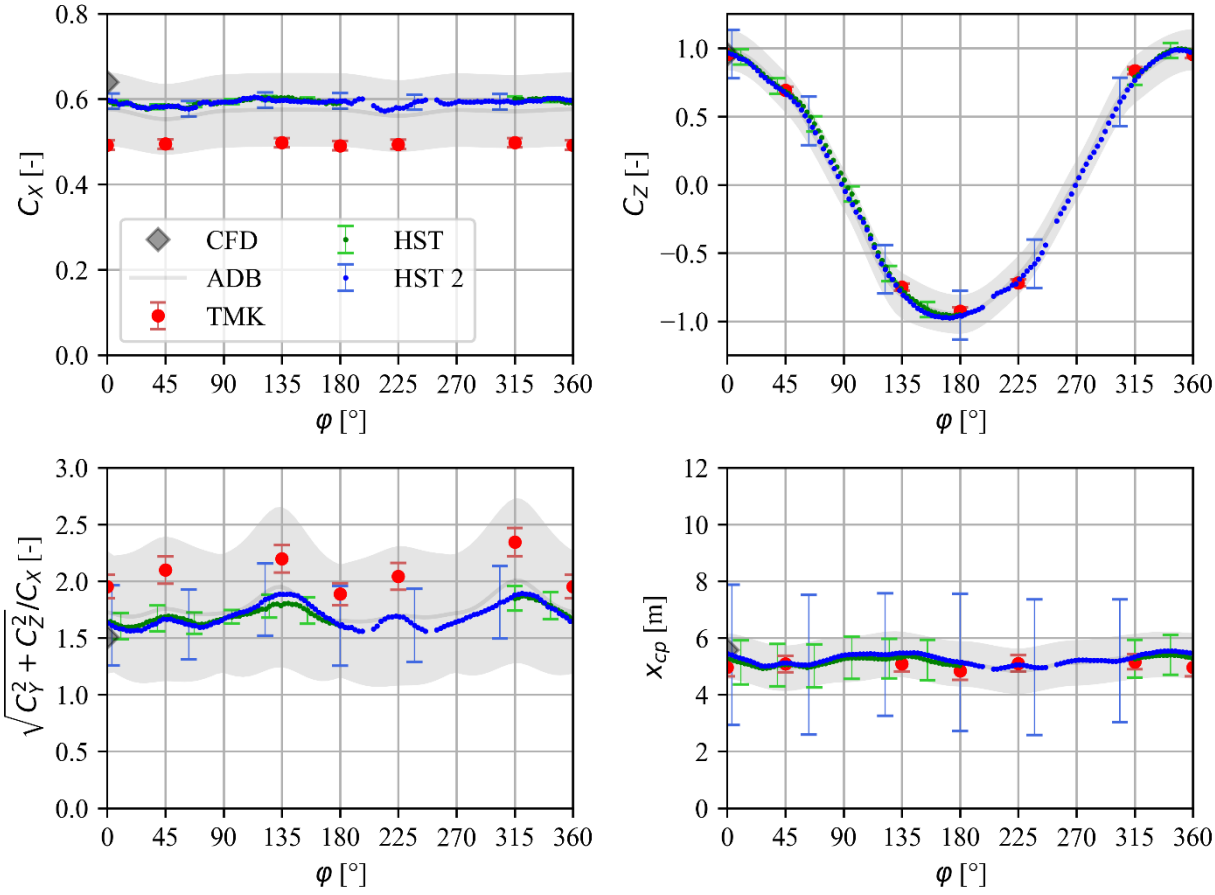

Figure 16: φ-polar

4. Conclusions

A huge experimental database for the CALLISTO flight experiment were created by means of wind tunnel measurements in the Trisonic Wind Tunnel (TMK) at the DLR in Cologne and the High-Speed Tunnel (HST) at the DNW in Amsterdam. Within this paper a detailed presentation of a small extraction of these data was given in order to give a rough overview on the aerodynamic coefficients and behavior of a VTVL configuration on the basis of the CALLISTO flight vehicle. In contrast to numerical simulation and the aerodynamic database, the continuously measurement allowed the assessment of flight conditions in-between the simulated flight conditions.
The focus was set on the comparison between the measurements in both wind tunnels and a very good agreement could be achieved between both wind tunnels for all the main aerodynamic parameters. An exception was the drag coefficient which was between 0.05 and 0.15 lower for the TMK as for the HST measurements in the presented dataset. A reason for this was not deducible from the data directly. Either slight differences of the wind tunnel models or mounting of the models in the wind tunnels (sting) seems plausible but would require a more detailed numerical or experimental investigation.
The nearly independency of the aerodynamic parameters within the relevant Reynolds number regime from the Reynolds number could be verified especially with the HST measurement. Here, the discrepancies of the parameters between the different Reynolds number are significantly lower than the uncertainty of the measurements and of the AEDB.
Finally, the investigation of the fins showed stability and controllability of the vehicle during descent and was to be found in a good agreement with the AEDB and numerical simulations.

Acknowledgment

The author thanks the technical staff of the TMK and HST wind tunnels for their support and technical expertise in conducting the experiments even under the complicated restrictions of the corona lockdown.

DOI: 10.13009/EUCASS2022-4634

References

[1] Dumont, E. et. al. (2021) *CALLISTO: A Demonstrator for Reusable Launcher Key Technologies.* Transactions of the Japan Society for Aeronautical and Space Sciences, Aerospace Technology Japan, 19 (1), Seiten 106-115. JSASS, DOI: 10.2322/tastj.19.106.

[2] Klevanski, J. und Ecker, T., Riehmer, J. and Reimann, B., Dumont, E., and Chavagnac, C. (2018) *Aerodynamic Studies in Preparation for CALLISTO - Reusable VTVL Launcher First Stage Demonstrator.* 69th International Astronautical Congress (IAC), 1-5 October 2018, Bremen, Germany. URL: https://elib.dlr.de/122062/

[3] Marwege, A., Riehmer, J., Klevanski, J., Gülhan, A., Ecker, T., Reimann, B. and Dumont, E. (2019) *First Wind Tunnel Data of CALLISTO - Reusable VTVL Launcher First Stage Demonstrator.* EUCASS 2019, 1. - 4. Juli, Madrid, Spain. URL: https://elib.dlr.de/128629/

[4] Marwege, A., Riehmer, J., Klevanski, J., Gülhan, A. and Dumont, E. (2019) *Wind Tunnel investigations in CALLISTO - Reusable VTVL Launcher First Stage Demonstrator.* 70th International Astronautical Congress (IAC), 21-25 October 2019, Washington D.C., United States. URL: https://elib.dlr.de/132566/

[5] Riehmer, J., Marwege, A., Klevanski, J., Gülhan, A. and Dumont, E. (2019) *Subsonic and Supersonic Ground Experiments for the CALLISTO VTVL Launcher Demonstrator*. International Conference on Flight Vehicles, Aerothermodynamics and Re-entry Missions & Engineering, 30.09.2019 - 03.10.2019, Monopoli, Italy. URL: https://elib.dlr.de/140709/